A novel inspection method for determining the cosmetic quality of automotive skin panels

Hazra S[1a], Roy R[a], Williams D[a], Aylmore R[b], Hollingdale D[c]

[a]Warwick Manufacturing Group, University of Warwick, Gibbett Hill Road, Coventry CV8 2PS UK
[b]Land Rover, Banbury Rd, Gaydon, Warwick, CV35 0RR, UK
[c]Jaguar Cars Limited, Abbey Road, Whitley, Coventry, CV3 4LF, UK

1. Introduction

The style and cosmetic quality of automotive skin panels creates desirability for the product and differentiates it from the competition. However, the geometry of certain styles may give rise to cosmetic defects, which reduces the perceived quality of panels. These defects do not hinder the functioning of the panel, but their appearance detracts from the intended styling and affects a customer's perception of the quality and value of the product.

A variety of cosmetic defects can occur as a result of the manufacturing process. One of the most common defects is a 'hollow', which is a 'dish-like' defect that occurs adjacent to functional features such as door handle depressions. According to Andersson, 2004, in cross section, a hollow has a sinusoidal shape with a depth of the order of about 100μm and is caused by the local springback in the panel. For example, Le Port et al., 2011 demonstrated that the defects observed in their test samples were caused by springback in the sheet by simulating the springback in the hemming process. It is difficult to identify a hollow in an unpainted panel but its presence becomes visually apparent after the application of paint because the glossy top-layer in a paint system makes the panel surface reflective. When painted, the hollow creates an optical distortion (Fig.1) because the geometry of the defect leads to varying focal lengths in the reflections from a panel (Hecht, 1998). A hollow can have a range of widths or wavelengths but Andersson, 2004, found the human eye is most

[1] Communicating author: Sumit.hazra@warwick.ac.uk

sensitive to the distortion caused by a hollow that is between 30 and 60mm wide. In flat geometries, the severity of the distortion was related empirically (Bartoe, 2001) but it can be determined quantitatively accordingly to the procedure outlined in ASTMC1652/C1652M, 2006. Bartoe, 2001, related the optical distortion in plate glass to its sinusoidal deviations from flatness with the following relationship:

$$D = 4\pi^2 W/L^2 \times 10^6 \quad (1)$$

where D is optical distortion in millidiopters, W is amplitude (mm) and L is wavelength (mm). Higher values of D are more noticeable to the eye.

Equation 1 suggests that the severity of a defect may be characterised by its wavelength and its depth. However, for panels with general curvature, a closed-form relationship between optical distortion severity and defect geometry does not exist and defect severity has to be determined visually. Panel inspections are carried out at several stages of the manufacturing process to enable potential problems to be traced and to identify the location and severity of defects. An important inspection is carried out after the stamping process when the cosmetic surface is first manufactured. At this point, the panel is unpainted, making it difficult to determine cosmetic quality because the surface of the panel is not reflective. As a result, the panel is usually prepared by ‘stoning’ with a whetstone or by applying highlighting fluid to simulate the reflectiveness of paint. ‘Stoning’ involves lightly scratching a panel with a whetstone to remove material. The quantity of material removed depends on the skill of the auditor, in particular the pressure applied on the panel with the stone. Defects that are concave in shape, such as hollows, remain unscratched and are highlighted because of its contrast with the surrounding scratched area. Highlighting fluid imitates the reflective properties of glossy paint so that the panel can be inspected visually with the aid of an inspection booth consisting of parallel strip lighting. The location and severity of defects is

determined by optical distortions, just as in the case for a painted panel. The manual preparation and inspection processes make panel assessment time consuming and subjective.

This paper describes the development and evaluation of a physically-based inspection method that uses the wavelet transform to identify defect-like shapes in panel topology that the human eye is specifically sensitive to and estimates their perceived severity. It is hoped that such a system will reduce the reliance on subjective audits carried out by auditors.

1.1 Inspection methods

Research into the identification of cosmetic defects can be broadly classified into the development of specialist measurement methods and the development of post-measurement techniques that objectively identify defects within measurement data. To reduce the subjectivity of preparation methods, particularly the stoning method, Reynolds et al., 1993 developed a specialist system to magnify defects using a double-pass retroreflection system. The system made it easier to identify defects by the human eye but it did not objectively locate a defect or rank its severity. To do this, post-measurement techniques, such as the wavelet transform (Hazra et al., 2008) and curvature analysis (Kase et al., 1999), were proposed. An important finding from the work carried out on post-measurement techniques was that they were capable of identifying defects from data obtained from conventional measurement instruments. For example, Le Port et al., 2011 and Shen et al., 2012 used stylus devices and Hazra et al., 2011 used a structured lighting system to identify defects. The ability of post-measurement techniques that work with widely available measurement methods suggested a promising basis for an inspection method for panels produced during serial production.

The most widely researched post-measurement method is the curvature analysis method. The method analyses the curvature change in a panel and highlights the presence of concave or

convex features. It is simple in concept but has two disadvantages. First, it relies on an optimised fit of the raw measurement data to calculate the local curvature of the panel. The data fit is required because the curvature calculation is sensitive to measurement 'noise' in the raw data and both Park et al., 2007 and Le Port et al., 2011 found that this 'noise' prevented the calculation of curvature. As a result they fitted their data with a second order polynomial (Park et al., 2007) and third order polynomial (Le Port et al., 2011) to smooth it out. The importance of the fit led Shen et al., 2012, in particular, to develop a specific algorithm that ensured that their data was optimally fitted. Second, the method locates concave features and identifies their depth but does not specifically identify concave features with the wavelengths that the human eye is most sensitive to. As a result, at their present state of development, they have not been used to predict the likely perceived severity of a defect. However, the technique has been demonstrated successfully to identify the location and depths of known defects in physical parts.

To locate and characterise the severity of a defect, the wavelet transform was proposed by Hazra et al., 2008 as an effective post-measurement method. They applied the technique to a part containing a cosmetic weld and a pre-production part containing minor and medium severity defects, as judged by trained auditors. A minor severity defect is classed as one which only a trained auditor will notice and a medium severity defect is classed as one which a particularly observant customer will notice. They found that this approach had two advantages. First, the multi-resolution property was able to identify the specific wavelengths, associated with a visible cosmetic defect, even when these defects were found in a curved panel. Second, the transform estimated the depths of the defects through a *correlation coefficient* (Section 2) and this value correlated to perceived severity. For example, medium severity defects returned a correlation value of -0.1 while minor severity defects returned a correlation value of -0.01. Hazra et al., 2011 also observed this relationship between the

correlation coefficient and perceived severity in a study involving a bodyside pre-production part containing four defects. However, a major disadvantage of the implementation described by Hazra et al., 2008 was that it analysed individual section profiles of a panel, which limited the examination to a small area of a panel.

This study applies the wavelet measurement concept proposed in Hazra et al., 2008 to data obtained with a structured lighting system to form an inspection process for cosmetic defects. An algorithm was first developed and implemented within Matlab v2009a for analysing the *surface* data from a GOM Atos structured lighting system. The algorithm was initially tested on two idealised geometries containing 0.05mm deep defects that were created within a CAD package. The algorithm was then tested on the surface data from the GOM system of five door panels that were obtained from successive stages of a stamping process. The output was compared to physical audits of the panels to determine the ability of the algorithm to locate and estimate the perceived severity of the defects contained within the panels.

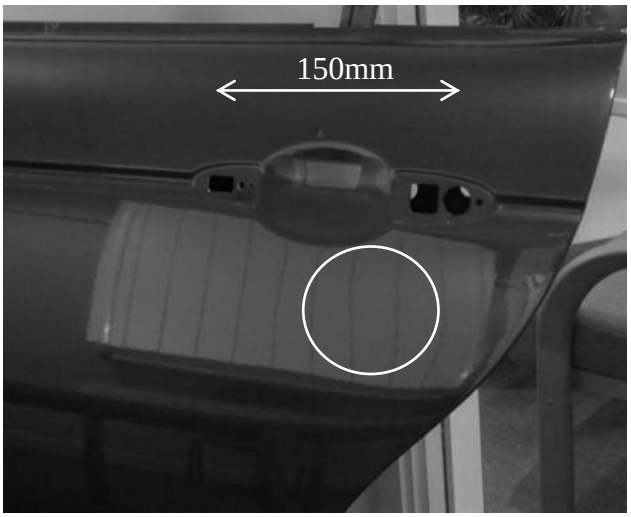

Fig.1 The reflection of parallel lines is distorted by the presence of a hollow in the circled region

2. Identifying the location, wavelength and depth of a defect

Figure 2 shows the cross-sectional profile of a panel containing a typical hollow defect.

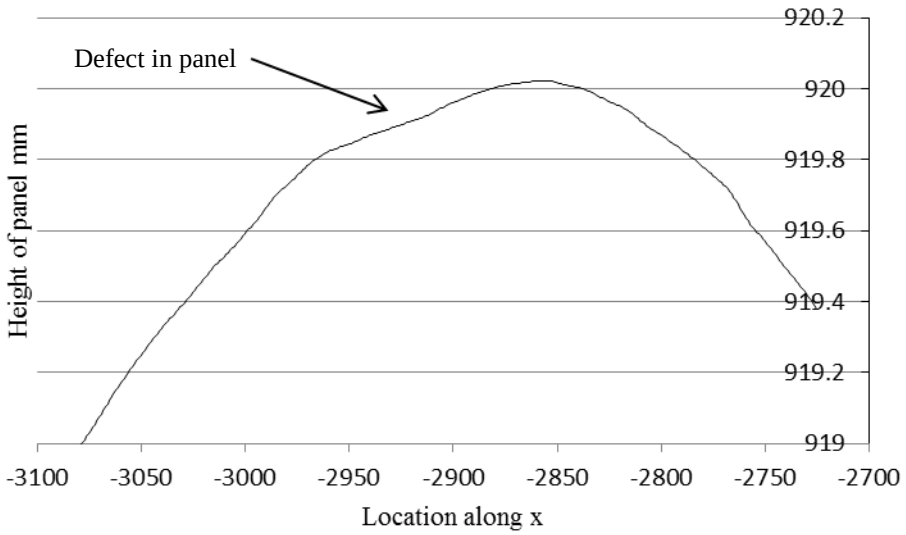

Fig.2 Cross-sectional profile of a panel containing a typical hollow defect.

It can be seen that the defect is approximately 50mm in width and the shape of the hollow and the surrounding panel is, qualitatively, made up of multiple wavelengths. The depth is of the order of 0.05mm to 0.1mm but its precise value depends on how depth is defined. For example, Le Port et al., 2011 chose to reference the depth of a hollow as the curvature of the panel changed from convex to concave (Fig.3a), whereas (Hu et al.,2008) used an algorithm that estimated depth from a simulated 'whetstone' spanning the highest points of the panel (Fig.3b).

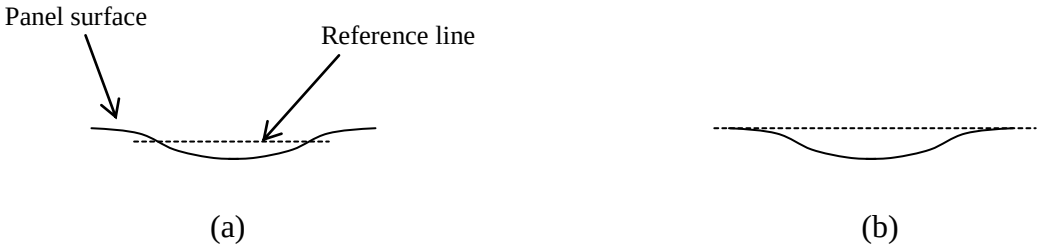

Fig.3 Shows two alternative reference lines from which depth of a defect is estimated. (a) shows a definition from Le Port et al., 2011 and (b) shows a definition from Hu et al., 2008

According to Burrus et. al, 1998, a function *f(x)* can often be better analysed if it is expressed as a linear decomposition by

$$f(x) = \sum_l a_l \psi_l(x) \tag{2}$$

where l is an index describing the length of the series, a_l are the expansion coefficients and $\psi_l(x)$ are functions that form the expansion set for x. A well-known example is the Fourier series

$$f(x) = \sum_{-l}^{l} b_l e^{-i\omega_l x} \tag{3}$$

where b_l are the expansion coefficients of the Fourier series and $e^{-i\omega_l x}$ is the sinusoidal expansion set and ω is its frequency. Using a wavelet function as the basis for the expansion, eq.(1) becomes

$$f(x) = \sum_{j,k} c_{j,k} \psi_{j,k}(x) \tag{4}$$

where

$$\psi_{j,k}(x) = 2^{j/2} \psi(2^j x - k) \tag{5}$$

ψ is a wavelet function, which forms the wavelet expansion set in eq.(4) and j is the *scale* of the wavelet function, which is analogous to the amplitude of the function and $c_{j,k}$ is the *correlation value*. The variable k controls the *translation* of the wavelet function in the x-direction (Fig.4). The shape and detail of *f(x)* is therefore represented by increasing ω in the fourier series (eq.3) and increasing j in the wavelet series (eq.4). However, a wavelet expansion set (eq.4) has the advantage that the wavelet function ψ is compactly supported (i.e

non-zero over a finite interval and zero elsewhere). This allows the *localisation* of the wavelengths in *f(x)* and makes it easier to identify *transient* events in *f(x)*. It should be noted that the fourier series locates frequencies (1/wavelength) in a function as well but it is difficult to extract this location information within the series. The wavelet series makes it easier because it is a two-dimensional expansion in *j* and *k* whereas the Fourier series is a one-dimensional expansion in *l* alone.

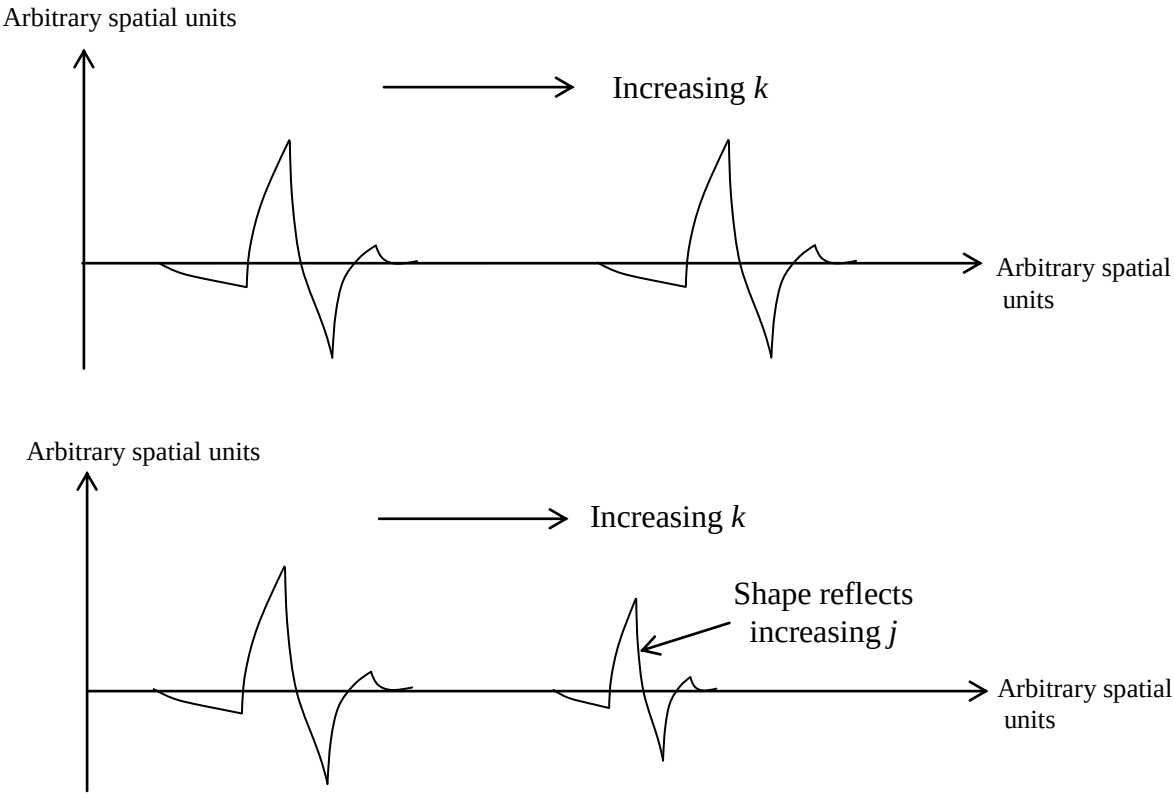

Fig.4 Schematic of the effect of increasing translation, *k*, and scale, *j*, of a wavelet from the 'coiflet' wavelet family. The design of the wavelet is described by Daubechies, 1994.

In the fourier series (eq.3), the expansion coefficients, b_l, are the amplitude of the sinusoidal expansion functions while in the wavelet series (eq.4), $c_{j,k}$, are known as correlation coefficients and are analogous to the amplitude of $\psi_{j,k}$. By calculating $c_{j,k}$ for the wavelengths that the human eye is sensitive to, the shape of a defect may be fully characterised. For expansion functions that are orthogonal ie.

$$\int \psi_l(x)\psi_{l+1}(x) = 0 \tag{6}$$

The a_l coefficients in eq.1 may be calculated with the convolution

$$a_l = \sum f(x)\psi_l \tag{7}$$

For a Fourier series, eq.6 becomes the Fourier transform:

$$b_l = \sum_{-l}^{l} f(x)e^{-i\omega_l x} \tag{8}$$

and for a wavelet series, eq.6 becomes the wavelet transform:

$$c_{j,k} = \sum_{j,k} f(x)\, 2^{j/2}\psi(2^j x - k) \tag{9}$$

From eq.9, the defect-wavelength that the human eye is sensitive to is fixed through j and $c_{j,k}$ is a dimensionless estimate of the depth of concave features that meet the wavelength criteria. In this way, the geometry of a defect may be fully characterised.

3. Identifying surface defects in a panel

The method described by Hazra et al., 2008 identified defects within individual cross-section profiles. Here, the wavelet concept is developed into an effective inspection system to assess the surface area of a panel. A five step algorithm was developed and implemented in Matlab 2009a with a graphical-user interface to speed up inspections. The five steps of the algorithm are as follows:

1. Surface data is imported into Matlab
2. The data is fitted using a cubic interpolation and re-sampled

3. Defect wavelength is assumed to be 60mm. The appropriate scaling value is calculated from the sampling period
4. The wavelet transform is carried out on the data using Matlab's '*cwt*' command
5. Negative and positive *c*-values of the wavelet result are plotted in the form of a contour plot and are superimposed on the original data.

In step 1, surface data, in the form of the 'ascii' file format is imported. In step 2, this data is re-sampled into a grid format (Fig.7). The imported surface data is, in general, randomly distributed, so in step 2, the data is re-sampled with a constant sampling period. Although the measurement data has to be fitted so that it can be re-sampled at a constant sampling rate, the quality of the fit that is required for the analysis is less critical that that required for a curvature analysis. This is because the analysing wavelength is larger than measurement noise, which has a small wavelength, low amplitude character. The wavelength difference makes the analysis less sensitive to measurement noise and as a result, the quality of the fit is not as critical as when it is used in curvature analysis. In step 3, the scaling value for the wavelet transform is calculated from Abry, 1997:

$$j = \frac{\lambda F_c}{\Delta} \tag{10}$$

Where λ is the analysing wavelength, F_c is the centre frequency of the daubechies wavelet and Δ is the sampling period in step 2. The centre frequency associates a wavelength to the daubechies wavelet (Fig.5) and Eq. 10 is essential in establishing the scale of the analysing wavelength.

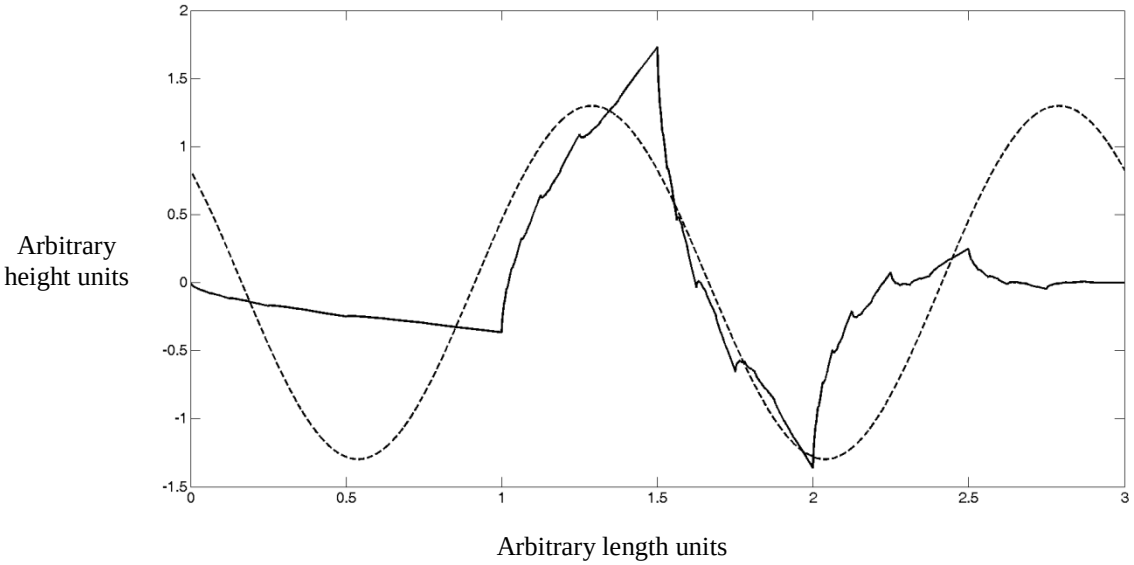

Fig.5 The solid line shows the daubechies 2nd order wavelet and the dotted line shows the wavelength that is associated with the wavelet. The wavelength is 1.5 arbitrary units

The analysing wavelength was chosen to be 60mm and this follows the finding of Andersson, 2004 that the human eye is sensitive to defects in the range of 30mm to 60mm. Smaller analysing wavelengths were investigated but these were found to identify the artefacts from post-processing the data collected by the structured lighting system (Section7.4). To minimise false-positives, the analysing wavelength was chosen to be 60mm. The sampling period in the data was chosen to approximately match the density of the data. Equation 10 shows that j is calculated by Δ for a given λ. On average, the sampling period for the five panels that were investigated was Δ=2.9mm and the scale used for the analysis was j=13.8. When sampling period changes, eq.10 adjusts j so that the c-value is unaffected. Fig.6 shows that changing the sampling period from 3.7mm to 1.4mm has a negligible effect on the identification of defects.

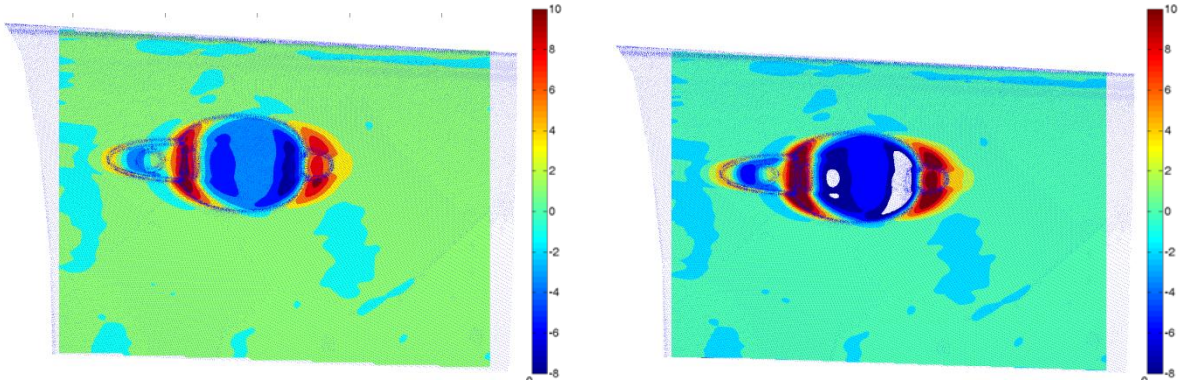

(a) (b)

Fig.6 Analysis of geometric data with sampling period of (a) 3.7mm and (b) 1.4mm

In step 4, the program carries out a looped 2D wavelet analysis along the grid of the re-sampled data (Fig.7). Correlation coefficients are calculated along the x-direction and then repeated for an incremental y-value.

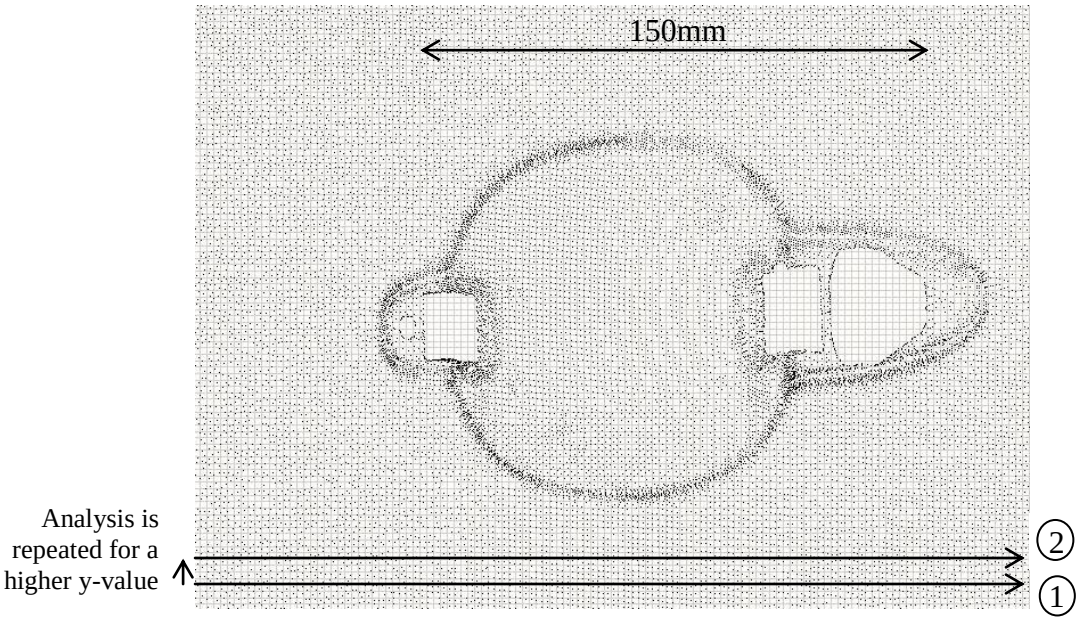

Fig.7 Image of scanned data from a door that has been fitted with a cubic interpolation. The black points represent data while the cubic interpolation is shown as the grey grid.

In step 5, the correlation coefficients are plotted as a contour map. Negative and positive coefficients are plotted separately and these refer to concave and convex features respectively. The results are plotted on the original data so that the location and severity of

defects may be identified visually. The severity of the defects was identified from the classification that was established in Hazra et al., 2011. In this classification, medium and minor severity defects have a *c*-value of the order or 0.1 and 0.01 respectively. Within an audit, a medium severity defect is one that may be identified by a critical customer while a minor defect is identifiable only by a trained auditor.

4. Wavelet analysis of ideal geometries

We followed Hazra et al., 2008 in using the daubechies 2nd order wavelet (Fig.5) for this study. The behaviour of the daubechies wavelet was assessed using two simple geometries. The first was a flat surface with a defect (Geometry A, Fig.8a) and the second was a curved surface with a radius of 1000mm (Geometry B, Fig.8b) containing a similar defect to Geometry A. The defect had a constant radius of 50mm and a depth of 0.05mm. To fulfil the combination constant radius of 50mm and depth of the defect, the width of the defect was about 10mm for Geometry A and 4mm for Geometry B rather than the 50mm that is observed in actual panels (Fig.2). At the edge of the defect, a fillet radius of 10mm was introduced to ensure a transition into the defect geometry. The three geometries were created in Solidworks, a commercial CAD software, and its IGES surface was meshed in DynaForm, a commercial finite element pre-processor. The surfaces were then analysed using the algorithm described in Section 3.

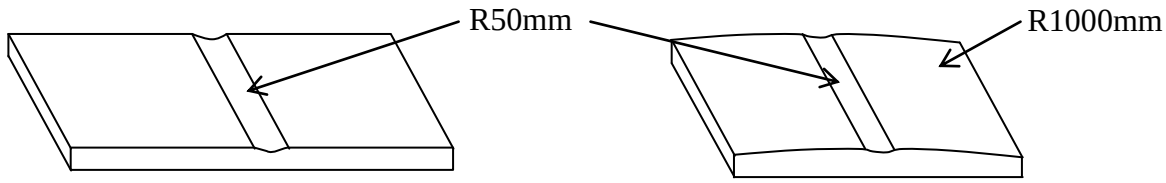

(a) Geometry A (b) Geometry B

Fig.8 (a) Flat and (b) curved (R=1000mm) geometries containing a 0.05mm deep defect (R = 50mm) used to test the behaviour of the daubechies wavelet.

4.1 Depth of defect

Geometry A (Fig.8a) was used to test the ability of the wavelet to detect a 0.05mm deep defect. The geometry was analysed with a 60mm wavelength wavelet.

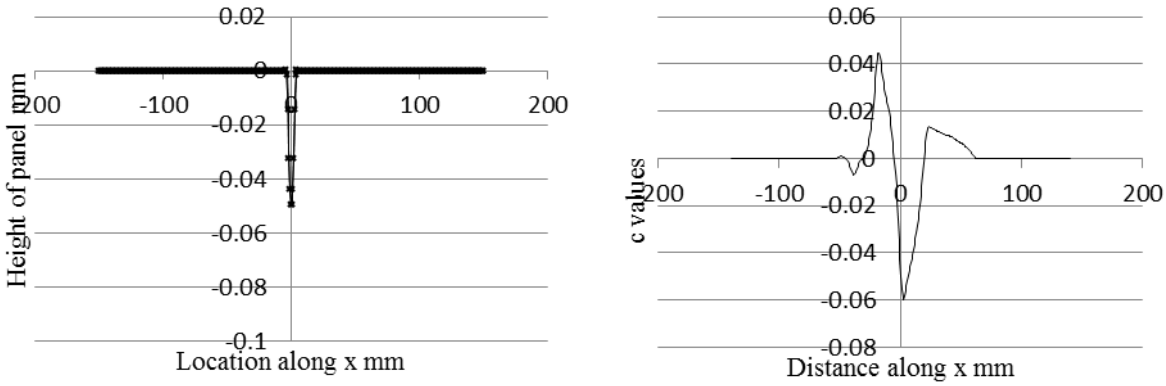

(a) (b)

Fig.9 (a) Cross-section of Geometry A, (b) $c_{j,k}$ values for the daubechies wavelet

Figure 9(a) shows the cross-section of Geometry A and the fit that was applied to the mesh created in DynaForm and Fig.9b shows the outcome of the wavelet transform analysis. It can be seen that the defect was detected with a *c* value of about -0.06 while the flat area outside the defect had a *c* value of 0. However, there was a large transition region beyond the defect where the *c*-value reached a maximum ($c \sim 0.04$ at x=-19mm and $c \sim 0.01$ at x= 21mm) before reducing to 0. This was partly due to the relatively sharp transition from the flat geometry into the defect geometry and the use of a 60mm wavelength to analyse a defect with a width of 20mm. Actual panels (Fig.2) have a more gentle transition into the defect so this behaviour is only observed in real panels near fillet radii (Section 7.2). However, the *c* value distribution was asymmetric and the negative *c*-value that is associated with the defect is offset by about 1mm to the right.

4.2 Effect of analysing-wavelength

The effect of the analysing wavelength was examined by comparing the result in Fig.9b to results obtained with a 20mm and 90mm wavelength.

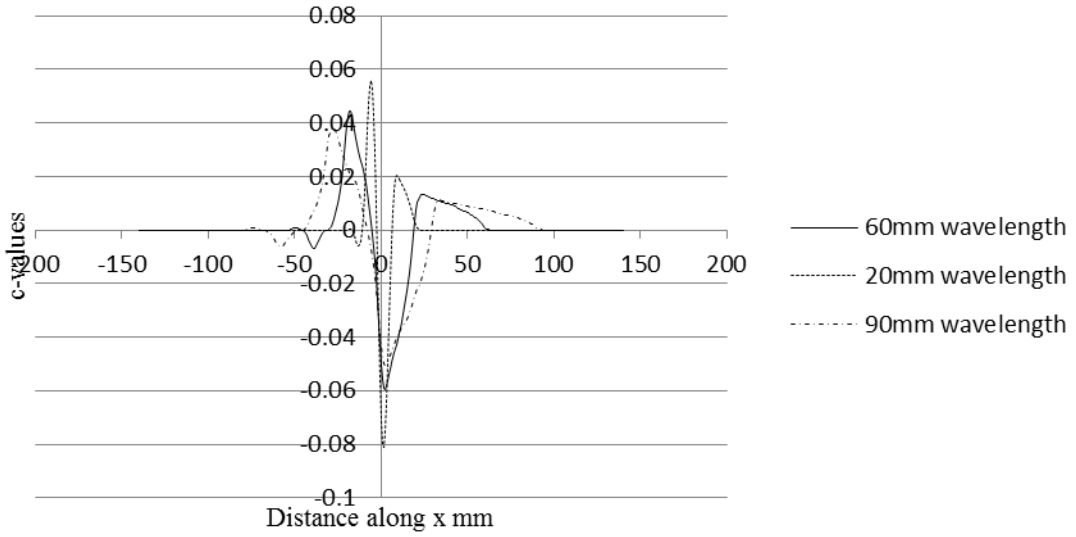

Fig.10 Effect of analysing wavelength on the detection of a defect

Figure 10 shows that when a 20mm wavelength is used, the *c*-value at the defect is smaller (*c* ~ -0.08) than the 60mm wavelength and the transition region is smaller. The transition region for the 20mm wavelength is between x=-6mm (*c*~0.05) and x=19mm (*c*~0.02). This indicated that the analysis becomes more sensitive as the analysing wavelength matches the size of the defect. Conversely, when a 90mm analysing wavelength is used, the *c*-value at the defect is greater (*c* ~ -0.05) than the 60mm wavelength and the transition region is larger.

4.3 The effect of panel curvature

The effect of panel curvature was investigated with Geometry B. Figure 11 shows the section profile data and the fit to the data. Figure 12 shows the analysis of the surface with a 60mm and a 10mm wavelet. The 60mm wavelet shows a *c*-value of 1.2 for most of the length of Geometry B with a transient deviation at the location of the defect. The 10mm wavelet was

chosen to match the 4mm width of the defect in Geometry B and the analysis shows that the *c*-values are 0.01 for most of the length of the section profile except at the location of the defect when *c*~-0.01. The comparison between the 60mm and 10mm wavelengths shows that the wavelet analysis becomes sensitive to the defect when the wavelength of the wavelet matches the size of the defect. When the wavelength is too large relative to the defect, the analysis is dominated by the overall panel curvature.

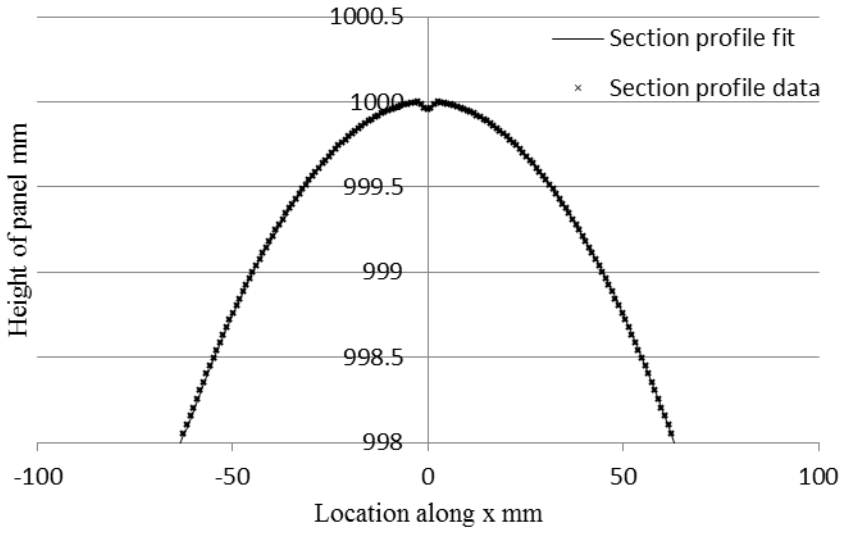

Fig.11 Section profile data and fit of Geometry B showing the 0.05mm deep defect

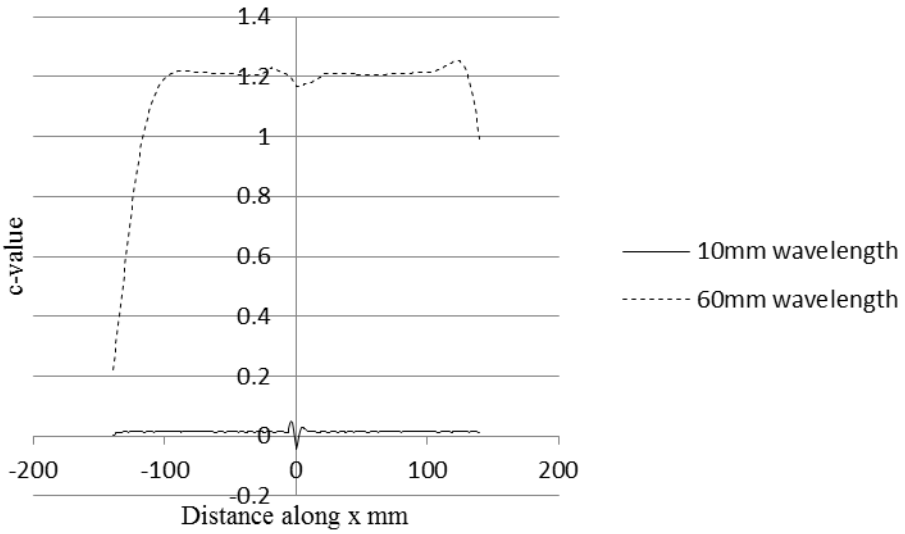

Fig.12 Effect of curvature and analysing wavelength on the detection of the 0.05mm defect

5. Measuring stage panels of a door part

The geometric data of a part that was input in step 1, Section 3, was obtained using a GOM ATOS 2e optical scanning instrument. The instrument utilises the structural lighting concept by projecting a parallel fringe pattern on a part and calculating the geometry of the part from the way its shape 'deforms' the fringes. The maximum uncertainty in the measurement of the scanner was quantified using VDI2634/3, 2008 and was determined to be ±0.03mm over a flat surface and the standard deviation error was determined to be 0.012mm.

The door was made from AA6111-T4 and this investigation focussed on defects that occurred around the door handle. The part was manufactured in five stages: the first was a draw stage while the second to fifth stages consisted of a combination of trim, flange and piercing operations. In the first stage, the main form of the part was pressed and the drawn shell was manufactured as a double attached part (Fig.13). The second and third operations consisted of trim operations to discard unwanted material in the blankholder and the walls of the drawn shell. The fourth and fifth operations involved flanging operations at the edge of the door in preparation for a future hemming operation of the outer skin to an inner reinforcement. Several piercing operations were also carried out in this stage to the door handle. For this investigation, only the left-hand side parts were investigated.

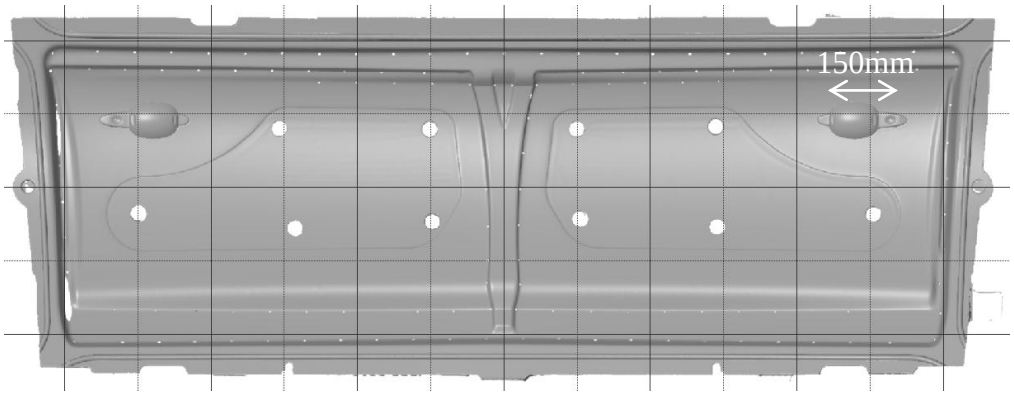

Fig.13 An optical scan of the draw die for the door panel. The door is manufactured as a double-attached part. The white circles were the air holes in the tool

Audits of all panels were carried out in a light booth containing vertical strips of light. Each panel surface was prepared with an oil-based 'highlighting fluid', to simulate the glossy finish of paint and inspected by a trained inspector. The location, severity and type of defect was marked on the panel. The most common type of defect was the hollow defect but the inspections also highlighted the presence of other types of geometric defects that were termed a 'ripple', 'high spot' and 'flat spot' by the auditor. A 'ripple' was a minor waviness or wrinkling in the panel, a 'high spot' was a distinct convex shaped defect and a 'flat spot' was a defect that did not have evident curvature.

6. Results

Overall, the wavelet and the audit analyses agreed in the location and evolution of the defects in the panel. Both analyses showed that the defects become less severe towards the end of the process (Figs.14 – 18). The cause of the evolution is discussed in Section 7.5.

6.1 Stage 1 of 5

In the first stage panel, the wavelet analysis highlighted four defects (Fig.14a). Defect 1 was a minor defect located along the left hand edge and defect 2 was a minor defect located at the bottom right-hand corner of the door handle. Defect 3 was a cluster of two minor defects located above the door handle and defect 4 was located on either side of the door handle. The analysis of convex defects (Fig.14c) shows two prominent defects, defects 8 and 9, on the cosmetic surfaces. Defect 8 is located at the top right corner of the door handle while defect 9 is located at the bottom left hand of the door handle. For clarity, the wavelet results presented in Figs.13 to 17 show concave and convex defects separately.

The physical audit of the panel showed five defects (Fig.14b). Defects A and B were similar to the locations of defects 1 and 2 in the wavelet analysis. Defect C was described as a minor ripple above the door handle depression and its location coincided with the cluster of defects

(defect 3) identified by the wavelet analysis, suggesting that defects located close together may appear as a ripple to the human eye. Defect E was a minor flat spot located at the right hand side of the door handle; the wavelet analysis did not identify this defect. Defect I was located above and to the right of the door handle and was classed as a medium severity 'high spot', or a pronounced local, convex feature and this coincided with the location of defect 8.

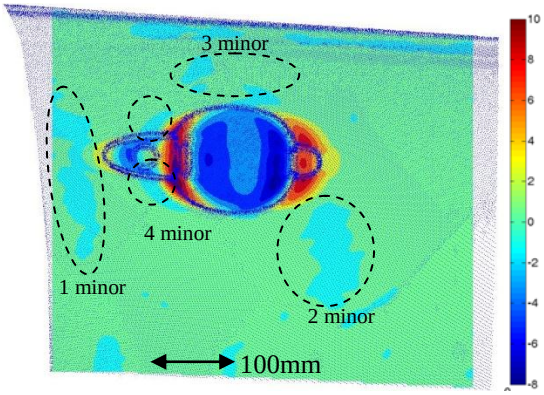

(a) Wavelet analysis concave surface

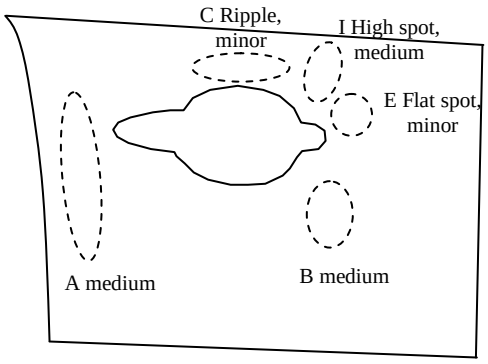

(b) Physical audit

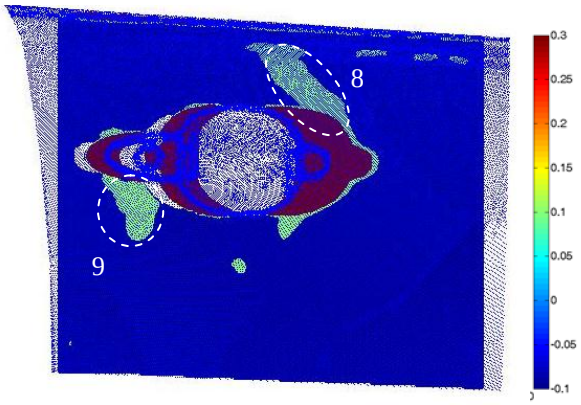

(c) Wavelet analysis convex surface

Fig.14 First stage door panel.

6.2 Stage 2 of 5

In the second stage panel (Fig.15), the audit analysis showed that defect A reduced in size and was classed a minor defect on this basis. Similarly, the equivalent defect 1 in the wavelet analysis showed a reduction in size and remained a minor defect. The audit indicated that all

other defects remained the same in location and severity. The wavelet analysis, however, showed three changes to the defects seen in stage 1. The first was that defect 2 split into two defects but this was thought to be a consequence of the scanning process. The size of the door meant that its geometry was scanned in stages and 'stitched' together by the scanning software. It was observed that the stitching process led to a local imperfection along the stitch that was not representative of the geometry's shape. This problem can be minimised by using a smoothing algorithm and the functioning of the algorithm is demonstrated in Section 7.4. The second change that was observed was the appearance of defect 5, which appears in a similar location to the audited defect E, although its location is not precisely the same. Lastly, the convex defect 9 grew in size diagonally from the door handle towards the bottom left hand corner of the panel.

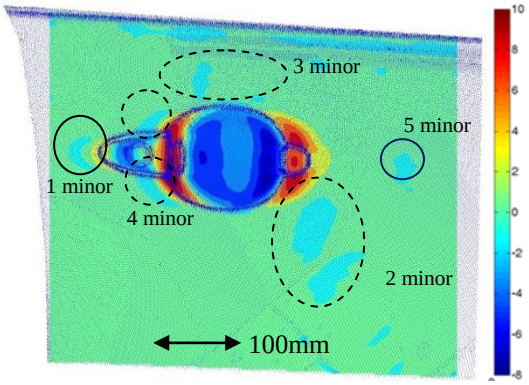

(a) Wavelet analysis concave surface

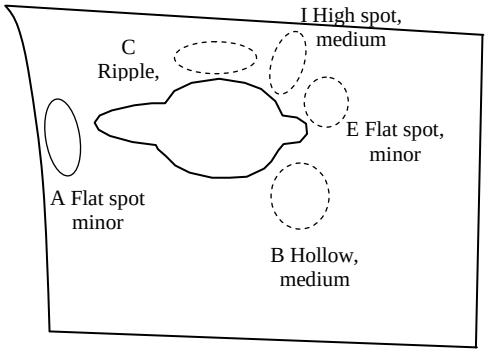

(b) Physical audit

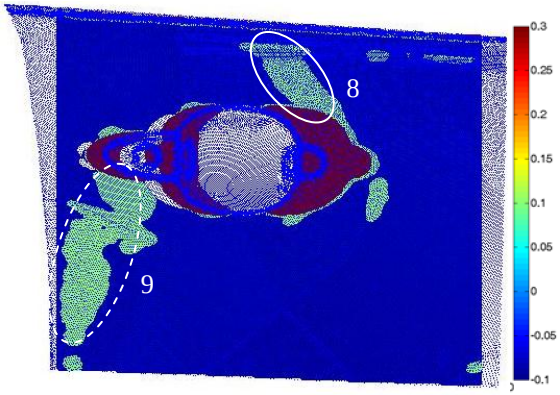

(c) Wavelet analysis convex surface

Fig.15 Second stage door panel.

6.3 Stage 3 of 5

In the third stage panel (Fig.16), the wavelet and audit analyses show defects in approximately equivalent locations. In the audit, there were two changes in the panel. First, defect B reduced sufficiently in size for its severity to be downgraded from medium to a medium/minor. Second, a new defect, defect F, appeared at the top left hand corner. In contrast, the wavelet analysis showed three changes. First, defect 3 reduced in size. Second, defect 5 became a cluster of defects. Third, a new defect, defect 6, appeared at the top right hand corner of the door handle. Defect F was not detected by the wavelet analysis and this is because the present implementation of the wavelet algorithm is unable to analyse corners that are not rectangular. Defect F was located outside the analysis area of the panel and was therefore not detected by the wavelet method.

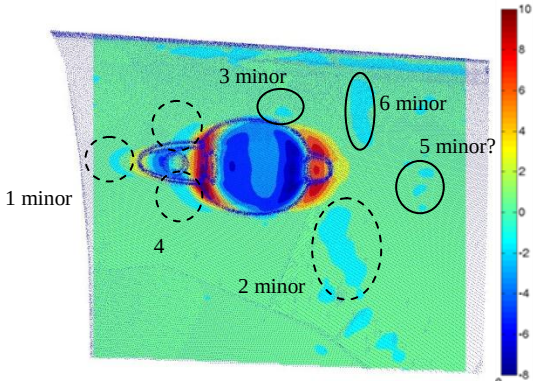

(a) Wavelet analysis concave surface

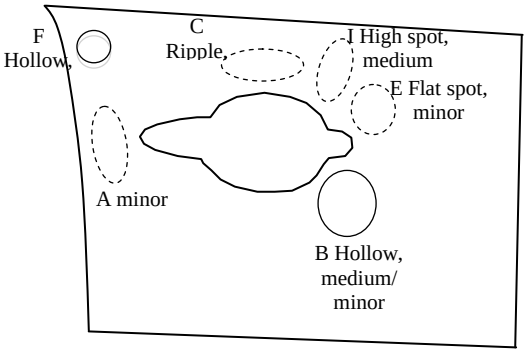

(b) Physical audit

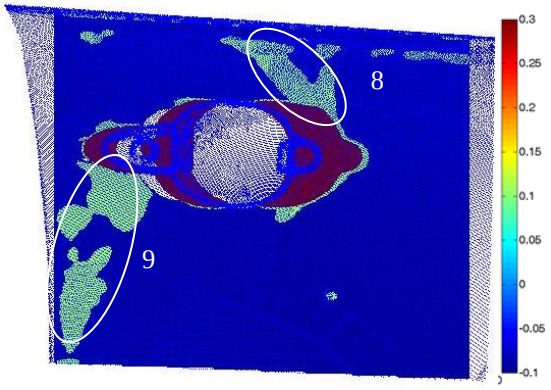

(c) Wavelet analysis convex surface

Fig.16 Third stage door panel.

6.4 Stage 4 of 5

In the fourth stage panel, the change to the wavelet results was to defects 3 and 9. Defect 3 changed shape and position above the doorhandle and defect 9 split into a separate defect 10 that was located along the left hand edge of the door. In the audit analysis (Fig.17b), the main change was the appearance of defect D, which became two defects located at the top and bottom of the door handle and corresponded to the location of defect 4 in the wavelet analysis.

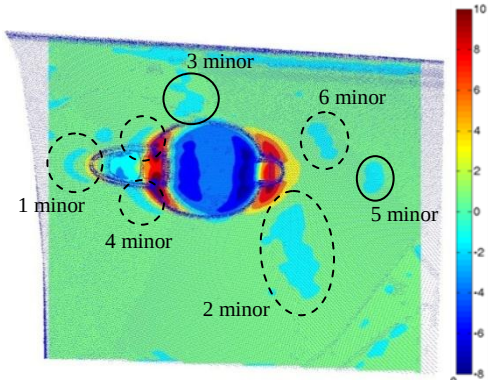

(a) Wavelet analysis concave surface

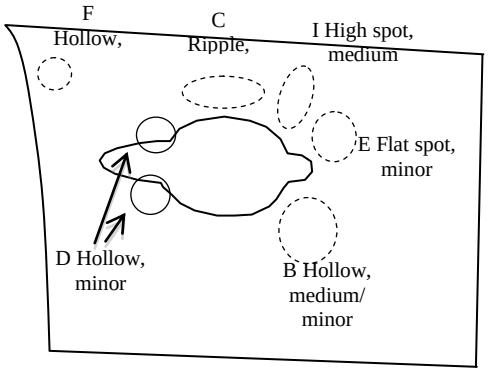

(b) Physical audit

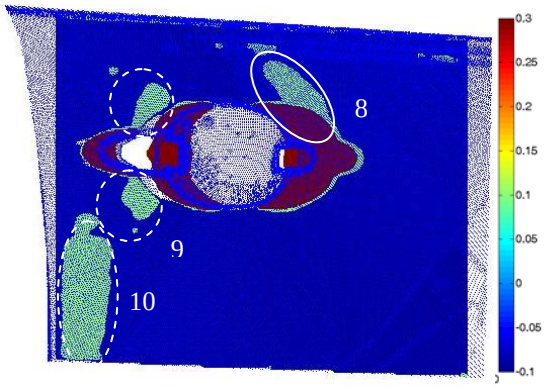

(c) Wavelet analysis convex surface

Fig.17 Fourth stage door panel.

6.5 Stage 5 of 5

In the fifth and final stage panel (Fig.18), the wavelet analysis indicated three changes. First, defect 3 changed in shape and moved slightly compared to the fourth stage panel. Secondly, defect 7 appeared at the bottom of the door handle depression and third, defects 9 and 10

combined into a single defect. In comparison, the audit showed two changes. First, defect B reduce in size and second, defect G appeared below the door handle depression in a similar location to defect 7 in the wavelet analysis.

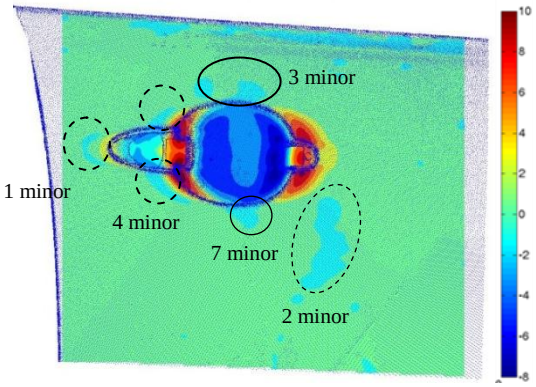

(a) Wavelet analysis concave surface

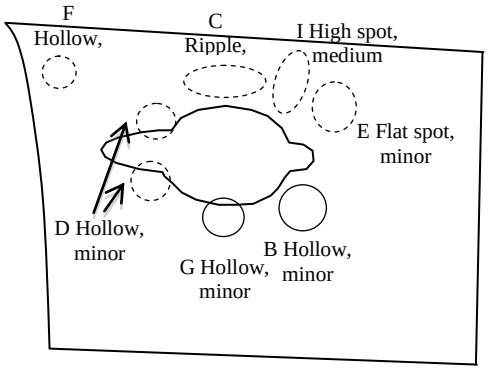

(b) Physical audit

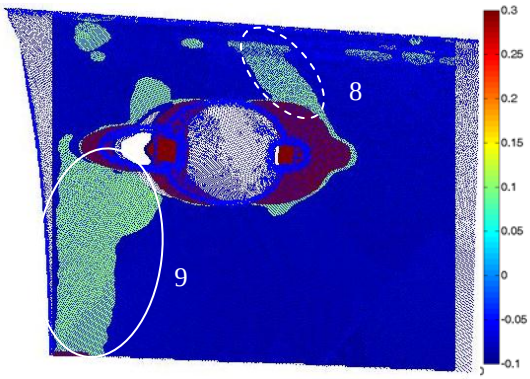

(c) Wavelet analysis convex surface

Fig.18 Fifth stage door panel.

7. Discussion

7.1 Comparison between the wavelet and audit analyses

The results of the wavelet and audit analyses are compared in Table 1 and several observations can be made. First, the number of defects identified by the wavelet and audit analyses and their locations were similar in all panels. For example, in stage 1, the wavelet analysis identified the hollow and convex defects identified by the audit analysis but failed to detect the ‘flat spot’ defect E. However, the wavelet analysis identified defects that were not

identified in the audit. For example, defect 4 was not identified by the audit analysis until stages 4 and 5 and the reason for this is discussed in section 7.2. Similarly, convex defect 9 was not identified by the auditor and its occurrence is discussed further in Section 7.3. Second, the severity of the hollow defects identified by the wavelet analyses was minor and the severity of the convex defects was medium, whereas the audit analyses identified a mixture of minor and medium severity defects in the panel. All the medium severity defects identified by the audit, apart from defect I, were due to their sizes or the area they covered on the panel. Since the wavelet analysis determines severity based on the depth of a defect rather than its size, it did not accurately reflect the severity of the defects in the door. The inclusion of defect size in the wavelet assessment of defect severity will be considered in future work. Third, defect F was not identified by the wavelet analysis because the present implementation of the wavelet method is unable to analyse corners that lie outside a rectangular analysis area. The development of an algorithm that can analyse more general panel shapes is left for future work. Overall, the degree of correlation between the wavelet and audit analyses shows the usefulness and promise of the wavelet algorithm in inspecting real, complex panels.

Stage	**Wavelet**	**Audit**
1	1 – minor	A – medium
	2 – minor	B – medium
	3 – minor	C – minor
	4 – minor	D - none
	not identified	E (flat spot) – minor
	8 (high spot) - medium	I (high spot) – medium
	9 (high spot) - medium	*not identified*
2	1 – minor	A – medium
	2 – minor	B – medium
	3 – minor	C – minor
	4 – minor	D - none
	5 – minor	E (flat spot) – minor
	8 (high spot) - medium	I (high spot) – medium
	9 (high spot) - medium	*not identified*
3	1 – minor	A – minor
	2 – minor	B – minor
	3 – minor	C – minor
	4 – minor	D - none
	5 – minor	E (flat spot) – minor

	6 – minor	*not identified*
	not identified	F – minor
	8 (high spot) - medium	I (high spot) – medium
	9 (high spot) - medium	*not identified*
4	1 – minor	A – minor
	2 – minor	B – minor
	3 – minor	C – minor
	4 – minor	D – minor
	5 – minor	E (flat spot) – minor
	6 – minor	*not identified*
	not identified	F – minor
	8 (high spot) - medium	I (high spot) – medium
	9 (high spot) - medium	*not identified*
	10 (high spot) - medium	*not identified*
5	1 – minor	A - none
	2 – minor	B – minor
	3 – minor	C – minor
	4 – minor	D – minor
	5 – none	E (flat spot) – minor
	not identified	F – minor
	7 – minor	G– minor
	8 (high spot) - medium	I (high spot) – medium
	9 (high spot) - medium	*not identified*

Table 1 Comparison between the results from the wavelet and audit analyses.

7.2 Effect of reversing the wavelet analysis

The analysis of Geometry A with a 60mm wavelength wavelet (Fig.9b) showed that the *c*-value distribution appeared to be offset by 1mm to the right. The asymmetry in the result suggested that analysis may be sensitive to the direction in which it is carried out. In Section 3, Fig.7 illustrated that the wavelet analysis is carried out from left-to-right. To assess the effect of the direction in which the wavelet analysis is carried out on the data that is input into the algorithm, the first stage panel was analysed in the reverse direction from right-to-left.

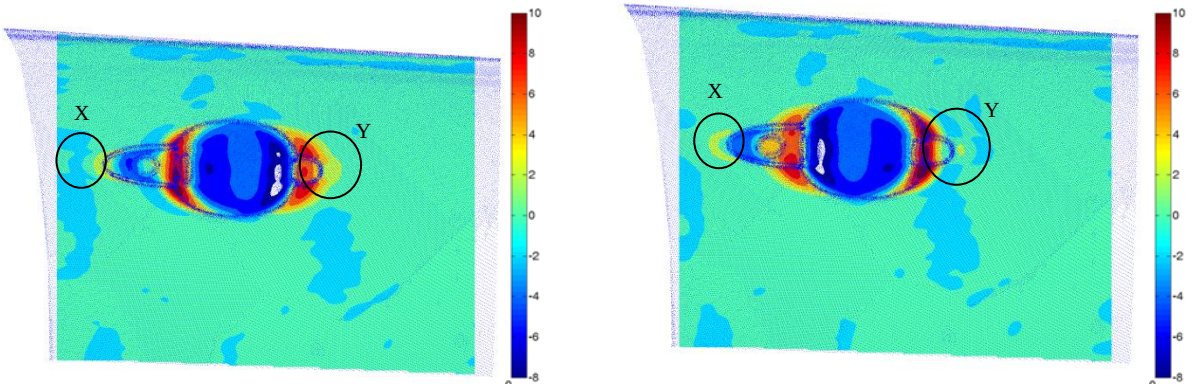

(a) left-to-right (b) reverse, right-to-left

Fig.19 Comparison of wavelet analysis comparing the direction of the analysis

The comparison shows that overall, the result remains similar. However, differences exist adjacent to the fillet radii, particularly in the areas marked X and Y. In Fig.19a, the left-to-right analysis shows a crescent-shaped defect in X, which does not appear in the reverse analysis (Fig.19b). Conversely, the reverse analysis (Fig.19b) shows three crescent-shaped defects in area Y that do not appear in the left-to-right analysis (Fig.19a). Defects 1, 2 and 3 were not affected by reversing the direction of the analysis. However, the reverse analysis highlights that defect 4 was an artefact of the direction of the analysis. It was therefore concluded that the defect D that was identified by the auditor for panels 4 and 5 were not detected by the wavelet analysis because the defect was too close to the fillet radii.

To reduce the effect of the direction of the analysis, an alternative mexican hat wavelet (Fig.20a) was tested on Geometry A because it is a symmetric wavelet (Daubechies 1994).

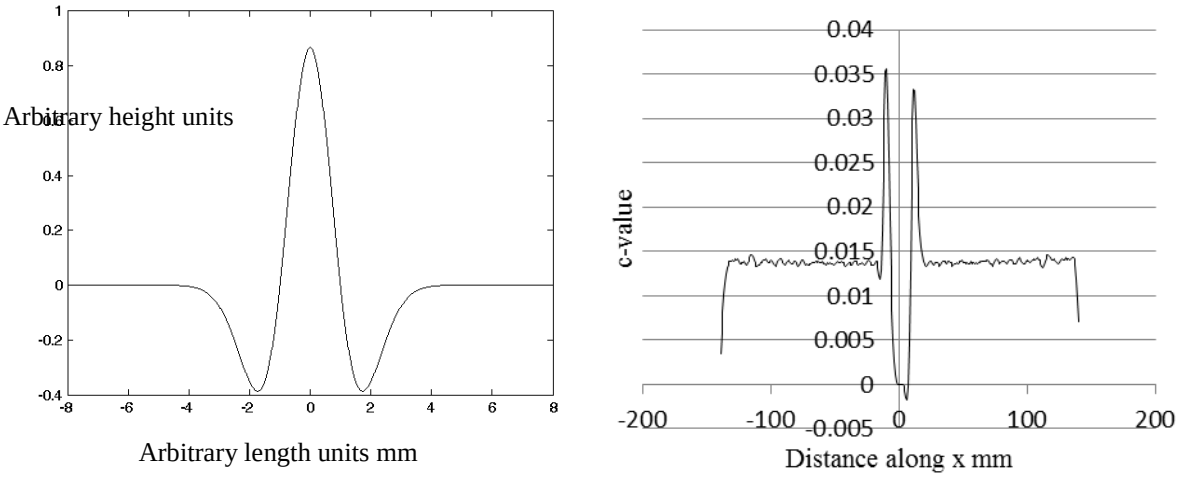

(a) (b)

Fig.20 (a) Appearance of the mexican hat wavelet and (b) analysis of Geometry C

Figure 20b shows the *c*-values that were returned from an analysis of Geometry C and that these are distributed more symmetrically about the location of the defect. However, the minimum value is higher (c ~ -0.001) than that of the daubechies wavelet (c ~ -0.01). When the wavelet is used to analyse the stage 1 panel, it can be seen that there is no effect from reversing the direction of the analysis (Fig.21(a) & (b)) and that the defect 1, 2 and 3 are still detected.

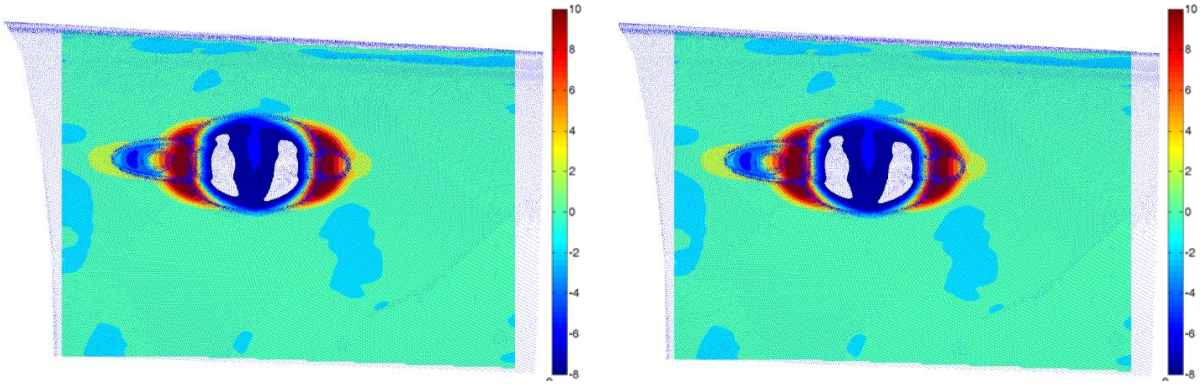

(a) left-to-right (b) reverse, right-to-left

Fig.21 Effect of analysis direction using the mexican hat wavelet

7.3 Evaluation of 'high-spots' in the panel

The audit analyses highlighted the presence of just one 'high-spot' or convex defect in all the panel stages (defect E, Figs 14-18) whereas the wavelet analyses identified the presence of two convex defects, defects 8 and 9 (Figs 14-18(c)). The location of defect 8 coincided with defect E in the audit and both analyses identified it in all the five panels. However, the wavelet analysis also identified an additional defect, defect 9, which was not identified by the audit. Fig.22 shows the cross-section of the first and fifth stage panels in the location of defect 9. It was evident that the left-hand edge of the fifth stage panel was more rounded compared to the first stage panel. Subjectively, the auditor did not identify the rounded shape as a defect in any of the stages and in this instance, the wavelet analysis identified a particularly convex topology as a defect.

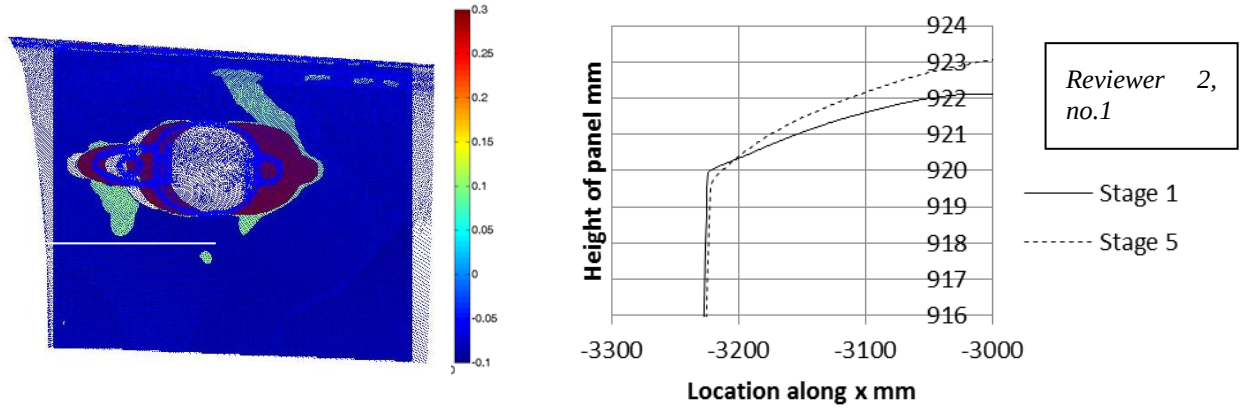

(a) Location of section profile in the first stage panel

(b) Comparison of panel shape in the first and fifth stage panels

Fig.22 Comparison of the section profiles corresponding to defect 9.

7.4 Effect of smoothing on the wavelet results

The size of the door panels (1.2m x 0.8m) was too large for its geometry to be captured by the optical scanner in one step. Instead, the geometry of the door was captured sequentially and 'stitched' together by the instrument's post-processing software without user

intervention. In cross-section, the 'stitch' can appear as a defect (Fig.23b) and can be highlighted by the wavelet analysis as a defect (Fig.23a).

To reduce the occurrence of this artefact, the analyses of the doors were smoothed by changing the defect-search wavelength from 60mm to 90mm. Figure 24 shows the effect of the smoothing.

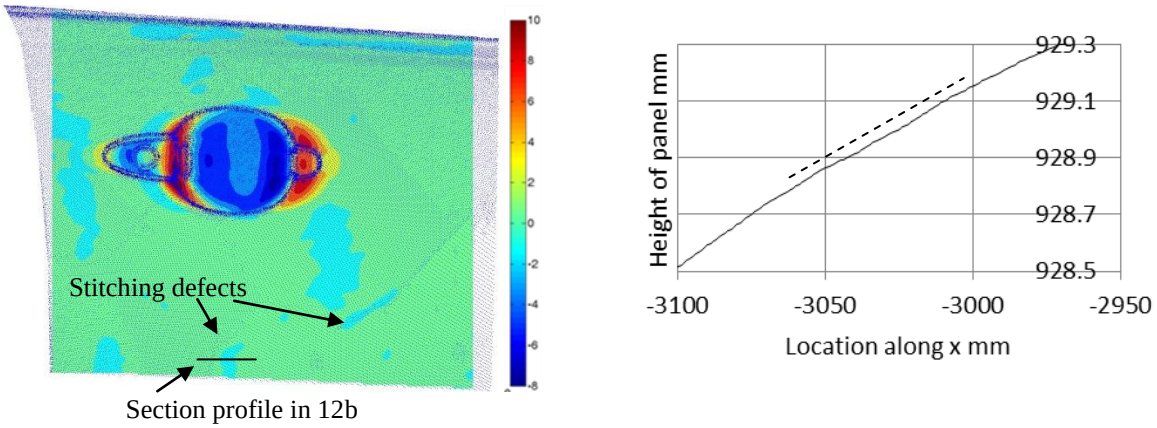

(a) First stage panel showing stitching defects (b) section profile showing the location of the stitching defect and a linear reference line

Fig.23 Figure showing the stitching defects from the optical scan.

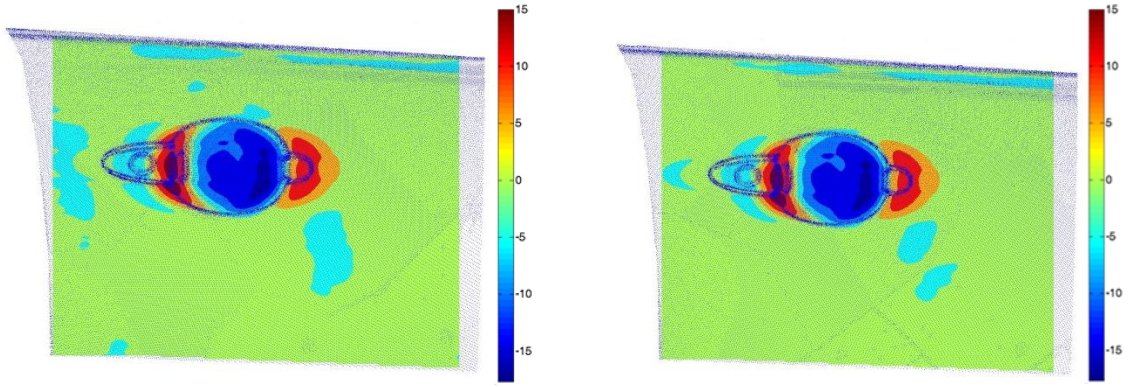

(a) Stage 1 (b) Stage 2

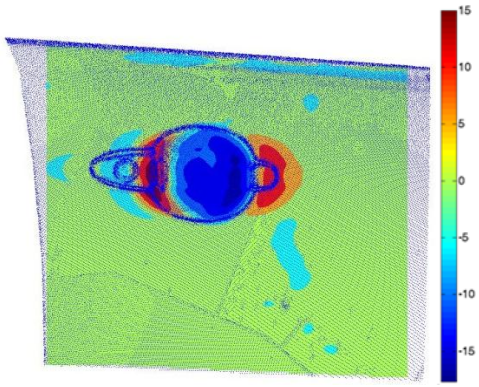

(c) Stage 3

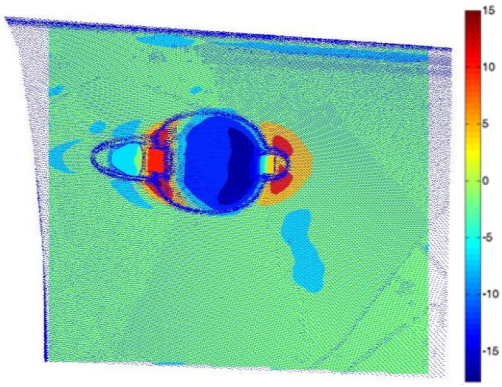

(d) Stage 4

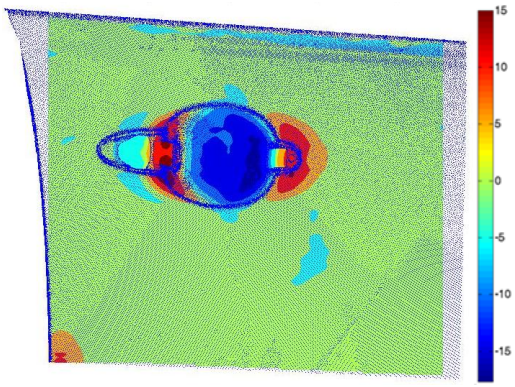

(e) Stage 5

Fig.24 Smoothing the wavelet results of Fig.14 to 18 by analysing for defects measuring 90mm in width.

Fig.24 shows that the smoothing reduced the occurrence of defects due to the stitching error but also made the analysis less sensitive to the smaller defects such as defects 4 and 5. The larger defects 1 and 2 remain and their evolution through the stages is still captured by the smoothed results. The overall results therefore, are a reasonable first-order estimation of the defects that were present in the panel.

7.5 Effect of stamping stages on the evolution of defects

The results of the wavelet analysis and the audit show clearly that the severity and location of defects in the door evolved and became smaller as the door went through the stages of the stamping process. In most cases, it was not possible to attribute the evolution to the

operations that were carried out since multiple operations took place at each stage. However, in the second stage operation, a large change to the size of defect 1 occurred following a trim operation on the panel adjacent to the defect (Fig.25). Because of the proximity of the trim operation to the defect, it is postulated that the trim led to a modification in the residual stress state in the defect location leading to a large reduction in the size of the defect.

The effect of the manufacturing stages implies that the quality of a panel does not just depend on its geometry but also on the process that is used to manufacture it. In the case of the door, the consequence of the process was to gradually reduce the size of the defects through the stages. However, it is equally conceivable that a different process could have led to defects of greater severity.

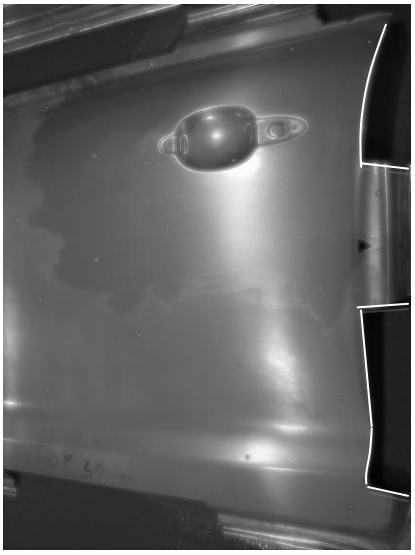

Fig.25 Second stage panel showing the trim operation that was carried out at the edge of the panel. White lines indicate the trim.

8. Conclusions

The aim of this study was to explore the development of an inspection system for cosmetic defects that does not require the intervention of a trained auditor. The inspection system that was proposed applied a defect detection concept outlined in Hazra et al., 2008 to geometric data acquired with a commercial structured lighting system. The concept of the inspection

system was implemented in an algorithm that was initially tested on two idealised geometries containing idealised defects. The analysis showed that the algorithm was capable of detecting defects with a 0.05mm depth when the analysing wavelet had a wavelength that matched the width of the defect. The algorithm was then tested on door panels obtained from each stage of a five stage stamping process and there were two outcomes. First, comparisons between the wavelet and audit analyses showed that the inspection system was capable of detecting the locations of both concave and convex defects in the panel. However, the algorithm was less successful at estimating the severity of the defects because within the algorithm, severity is determined by the depth of the defect for a given wavelength. On this basis, the algorithm estimated all the defects to be minor, except for the convex defect, defect 8, which was judged to be of medium severity. However, the auditor assessed defects such as defect 1 and 2 to be of medium severity because of their size. Incorporating this parameter into the algorithm will be for future work. Second, the daubechies wavelet shows a dependency on the direction that the analysis is carried out. However, it was demonstrated that changing the choice of wavelet to the 'mexican hat' wavelet eliminates this reversibility. However, because the 'mexican hat' wavelet produces different *c*-values to the daubechies wavelet, its output will have to be calibrated to the severity of known defects. The third conclusion is that the design of the stamping process can influence the number of defects and their locations and severity in a part. The number of defects and their severities was seen to reduce through the stages so that the quality of the door improved. Overall, the study demonstrates a promising framework for an inspection process that minimises the reliance on subjective audits carried out by specialist auditors.

9. Acknowledgements

The authors gratefully acknowledge the financial support provided by Advantage West Midlands, the European Regional Development Fund and Jaguar Land Rover. The audits were carried out by Mr. Eddie Burke.

10. References

Abry, P., 1997. Ondelettes et turbulence. Multirésolutions, algorithmes de décomposition, invariance d'échelles. Diderot Editeur, Paris.
Andersson, A., 2004. Macro-Geometric Defects - A numerical and experimental study of springback and surface defects, Department of Production and Materials Engineering. Lund University, Lund.
ASTMC1652/C1652M, 2006. Measuring distortion in flat glass products using digital photography of grids,.
Bartoe, R., 2001. The dynamics of ceramic rollers and operating and maintenance practices to produce quality tempered glass., Proceedings of the Glass Processing Days.
Burrus, C.S., Gopinath, R.A., Guo, H., 1998. Introduction to Wavelets and Wavelet Transforms: A primer, Prentice-Hall Inc., New Jersey.
Daubechies, I., 1994. Ten lectures on wavelets, Society for Industrial and Applied Mathematics, 61, p.75
Gabor, D., 1946. Theory of communication. Journal of the Institute of Electrical Engineers 93(III), 429-457.
Hazra, S., Williams, D., Roy, R., Allen, M., Hollingdale, D., 2011. Predicting the Occurrence of Cosmetic Defects in Automotive Skin Panels, In: Menary, G. (Ed.), 14th International ESAFORM Conference on Material Forming. American Institute of Physics, UK, p. 253.
Hazra, S., Williams, D., Roy, R., Aylmore, R., 2008. Detecting subtle cosmetic defect in Automotive skin panels. Proc. IMechE Part C: J. Mechanical Engineering Science 222, 2203.
Hecht, E., 1998. Optics. Addison Wesley, Harlow.
Hu, Y., Zhu, X., Lee, W., 2008. Surface low prediction with LS-DYNA and Dynaform, In: Hora, P. (Ed.), Proceedings of the 7th International Conference and Workshop on Numerical Simulation of 3D Sheet Metal Forming Processes. Institute of Virtual Manufacturing, ETH Zurich, Interlaken, Switzerland, pp. 779-785.
Hubbard, B., 1996. The world according to wavelets. AK Peters Ltd., Wellesley, MA.
Kase, K., Makinouchi, A., Nakagawa, T., Suzuki, H., Kimura, F., 1999. Shape error evaluation method of free-form surfaces. Computer Aided Design 31, 495 - 505.
Le Port, A., Thuillier, S., Manach, P.-Y., 2011. Characterization of surface defects after flanging of metallic sheets. Journal of Materials Processing Technology 211, 2062.
Mallat, S., 1999. A wavelet tour of signal processing. Academic Press, London.
Park, C., Chung, W., Kim, B., 2007. A numerical and experimental study of surface deflections in automobile exterior panels. Journal of Materials Processing Technology 187 - 188, 99-102.
Reynolds, R., Karpala, F., Clarke, D., Hageniers, O., 1993. Theory and applications of a surface inspection technique using double-pass retroreflection. Optical Engineering 32, 2122 - 2129.

Shen, H., Li, S., Chen, G., 2012. Quantitative analysis of surface deflections in the automobile exterior panel based on a curvature deviation method. Journal of Materials Processing Technology 212, 1548-1556.
VDI2634/3, 2008. Optical 3D measuring systems: multiple views systems based on area scanning.